JOURNAL OF MATERIALS SCIENCE 23 (1988) 713–717

Thermal cycling of tungsten-fibre-reinforced superalloy composites

ROBERT C. WETHERHOLD
Department of Mechanical and Aerospace Engineering, State University of New York, Buffalo, New York 14260, USA

LEONARD J. WESTFALL
Advanced Metallics Branch, NASA–Lewis Research Center, Cleveland, Ohio 44135, USA

The thermal cycling of a tungsten-fibre-reinforced superalloy (TFRS) composite is typical of its application in high-temperature engine environments. The mismatch in thermal expansion coefficients between fibre and matrix causes substantial longitudinal (0°) stresses in the composite, which can produce inelastic damage-producing matrix strains. The case of thermal fatigue is explored as a "worst case" of the possible matrix damage in comparison with specimens which are also mechanically loaded in tension. The thermally generated cyclic stresses and the attendant matrix plasticity may be estimated using a non-linear finite-element program by proposing a physical analogue to the micro-mechanics equations. A damage metric for the matrix is proposed using the Coffin–Manson criterion, which metric can facilitate comparisons of damage among different candidate materials, and also comparisons for a given material subjected to different temperature cycles. An experimental programme was carried out for thermal cycling of a 37 vol% TFRS composite to different maximum temperatures. The results confirm the prediction that thermal cycling produces matrix degradation and composite strength reduction, which become more pronounced with increasing maximum cyclic temperature. The strength of the fibre is shown to be identical for the as-fabricated and thermally cycled specimens, suggesting that the reduction in composite strength is due to the loss of matrix contribution and also to notching effects of the matrix voids on the fibre.

1. Introduction

There are a number of applications in aerospace structures, propulsion systems and heat engines which require durable, high-temperature materials. The improvements possible in monolithic nickel- and cobalt-based superalloys have reached the incremental stage; there is a need for materials which offer a basic improvement in high-temperature properties. Composite materials such as tungsten-fibre-reinforced superalloys (TFRS) offer such a basic improvement [1, 2]. At high use temperatures, this composite is a ductile fibre–ductile matrix system, alleviating many of the notch sensitivity problems encountered with brittle systems.

Many of the high-temperature applications involve a cyclic temperature field. Composites are composed of constituents which possess different thermal expansion coefficients and moduli. Under the cyclic temperature field, the constituents can develop considerable longitudinal (0°) stresses. This is due to a good fibre–matrix bond which enforces longitudinal strain compatibility during expansion in the face of mismatched thermal expansion behaviour. Damage of composites has been observed in a number of materials systems subjected to cyclic temperature fields [3–5]; this is most severe for a highly mismatched system such as C–Al [5]. If the cycle occurs over a short time, the behaviour of the matrix is elastic–plastic, while the fibre remains elastic. This offers the possibility of stress–strain analysis similar to that employed by Garmong [6–8] and other authors [4, 9, 10]. In addition, the matrix damage per cycle may be predicted and qualitatively assessed.

In this work, the background for prediction of deformation and relative damage is reviewed, and predictions are made for TFRS composites. An experimental programme of short-time thermal cycling is performed, and various measures are taken of the matrix degradation. The effect of thermal cycling damage on composite and fibre strength is then assessed.

2. Stress analysis

The longitudinal stress and deformation response of the constituent fibre (f) and matrix (m) of an aligned fibre composite may be approximated by solving the following system of one-dimensional equations:

$$\dot{\varepsilon}_f = \dot{\varepsilon}_m \tag{1}$$

$$\dot{\varepsilon}_f = \frac{\dot{\sigma}_f}{E_f} + \alpha_f \dot{T}$$

$$\dot{\varepsilon}_m = \frac{\dot{\sigma}_m}{E_m} + \alpha_m \dot{T} + \dot{\varepsilon}_p \tag{2}$$

$$\dot{\sigma}_f A_f + \dot{\sigma}_m A_m = \dot{P} \tag{3}$$

0022–2461/88 $03.00 + .12

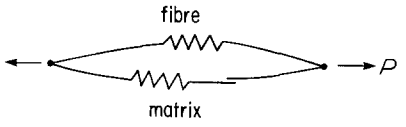

Figure 1 Model for longitudinal deformation.

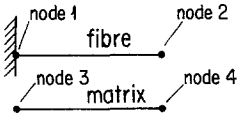

Figure 2 Finite-element representation of deformation model. Equivalent nodes: (1, 3), (2, 4).

where $(\dot{})$ = d/dt; A_i = area or volume fraction for constituent i, P = external applied axial load and E_i, α_i are the instantaneous Youngs' modulus and thermal expansion coefficient, respectively, for constituent i.

This model may be pictured as in Fig. 1 if we assume perfect plasticity in the yielded matrix. It is assumed that there is sufficient fibre volume fraction to avoid fibre plasticity with its attendant racheting (permanent cyclic set); this is reasonable for structural composites. The resulting deformation under these conditions is called "captive plastic cycling" of the matrix [9]. The material properties as functions of temperature are given in Table I. It is assumed that the amount of time spent at high temperature in rapid thermal cycling is insufficient to cause substantial creep. Since there are only elastic and plastic deformations, the deformation rate is homogeneous of order unity in stress rate, and the time scale is irrelevant. For our case of thermal fatigue, the applied load $P = 0$. The responses of the constituents and the system are driven by the mismatch in thermal expansion coefficients, and the required strain compatibility of the consitituents.

The system of rate equations (Equations 1 to 3) may be integrated by use of the MARC (MARC Analysis Research Corp., Palo Alto, CA, 1986) non-linear finite-element program. The stresses and strains were obtained by using beam/column elements (MARC element No. 5) for the fibre and matrix, and constraining their action as in Fig. 2. This represents a novel use of MARC to use physical analogues (beams) to solve the micro-mechanics equations. One end is fully constrained, and the other is free and unloaded, since there are no applied loads; $P = 0$. The beam rotation is not utilized, since the two beams possess equivalent end-nodes. The stress and strain state in each beam is homogeneous, and the instantaneous temperature is the same for both beams. The relative volume fractions of fibre and matrix are set by the cross-sectional areas of the beam/column elements. The two elements are shown separately for clarity in Fig. 2; they actually are one-dimensional, and occupy the same space.

After cool-down to 20° C from the approximate stress-free temperature of 920° C, the temperature is increased to the maximum and then cycled (see Fig. 3 for the temperature history). The low cyclic temperature of 430° C represents an engine cycling condition. The resulting stresses in the fibre and matrix, and the matrix plastic strain, are given as a function of cyclic temperature in Fig. 4, for T_{max} = 1000° C.

The matrix stress and plastic strain are two key variables which are found by the analysis. The fibre stress may be determined from the matrix stress using Equation 3, and the matrix plastic strain has import for the damage sustained by the matrix. During the first part of cooldown A to B (Fig. 4), the matrix contracts more than the fibre, resulting in positive stress increments during elastic unloading from plasticity. Due to the low yield at high temperature, the matrix yields in tension almost immediately, and stays in yield from B to C. During the temperature reversal from C to D, the stress increment is negative as elastic unloading from plasticity occurs. At the D the yield stress is reached, and subsequent stress values must decrease from D to A due to the decrease in yield stress as temperature increases. The portions of the curve where plasticity occurs show changing values of matrix plastic strain; where plastic strain is constant, elastic unloading is occurring. It is Fig. 4 which suggests that the addition of an applied tensile load may decrease the matrix cyclic plastic strain, and thus decrease the damage, by limiting the yielding during the segment DA. The case of only thermal fatigue may be expected to be a "worst case" for damage; while this has not been calculated, it has been observed [13].

3. Matrix damage metric

During thermal cycling, the matrix experiences a cyclic plastic strain, which causes damage. The matrix is coupled with stiff fibres which inhibit its free expansion. This suggests the application of the Coffin–Manson (CM) equation, which was developed for

TABLE I Material properties*

Property	Reference	Data range (° C)	Units
Fibre			
$E = (400 - 0.04T)10^9$	[11]	20 to 1100	Pa
$\nu = 0.29$	Estimate	–	–
$\alpha = 4.44 \times 10^{-6} + 8.87 \times 10^{-10}T$	[12]	20 to 1127	$(°C)^{-1}$
$Y = 0.7 \times 10^{**} (9.33 - 1.26 \times 10^{-4}T - 2.88 \times 10^{-7}T^2)$	[13]	20 to 1000	Pa
Matrix			
$E = (204.3 - 8.27 \times 10^{-2}T)10^9$	[14]	20 to 980	Pa
$\nu = 0.30$	Estimate	–	–
$\alpha = 7.07 \times 10^{-6} + 14.09 \times 10^{-9}T$	[13]	20 to 1100	$(°C)^{-1}$
$Y = 10^{**} (8.49 + 4.36 \times 10^{-4}T - 1.75 \times 10^{-6}T^2)$	[15]	20 to 1000	Pa

*All temperatures T in °C; Y is yield, ** implies an exponentiation.

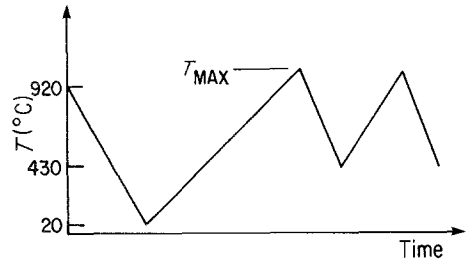

Figure 3 Cyclic temperature history.

constrained materials [16, 17], to the matrix:

$$\Delta\varepsilon_p N^{1/2} = C \quad (4)$$

where $\Delta\varepsilon_p$ = matrix cyclic plastic strain, N = cycles to failure and C = material constant. The outright failure of a constrained material is problematic, since there is no way to directly observe its failure. We may rather suggest a damage metric based on the CM equation:

$$\frac{\Delta\varepsilon_p n^{1/2}}{C} = D \qquad D\varepsilon\,[0, 1] \quad (5)$$

where D = damage metric, equal to 1 at "failure" and n = number of cycles, $n \leqslant N$.

The use of Equation 5 implies that if $\Delta\varepsilon_p$ is computed (by use of the MARC program) and C is known from experiments, that we have a method of gauging the relative matrix damage for different materials and loading conditions. For example, if two matrix materials are under consideration, the relative number of cycles to the same degree of damage is

$$\frac{n^{(1)}}{n^{(2)}} = \left(\frac{\Delta\varepsilon_p^{(2)}}{\Delta\varepsilon_p^{(1)}}\frac{C_1}{C_2}\right)^2 \quad (6)$$

where $n^{(i)}$, $\Delta\varepsilon_p^i$ and C_i are the number of cycles, cyclic plastic strain and material constant, respectively, for Material i.

Alternatively, with one material subjected to different thermal (or thermomechanical) cycles, this ratio of the number of cycles to equivalent damage becomes

$$\frac{n^{(1)}}{n^{(2)}} = \left(\frac{\Delta\varepsilon_p^{(2)}}{\Delta\varepsilon_p^{(1)}}\right)^2 \quad (7)$$

For the thermal cycle used here, the cyclic plastic strain and the ratio of number of cycles to equivalent damage are given for different maximum cyclic temperatures in Table II for a 40 vol % W system. The damage per cycle is thus predicted to rise sharply with increasing maximum temperature. It takes 325 cycles at 850° C to produce as much damage as 100 cycles at 1000° C, compared with only 62 cycles at 1090° C.

4. Experimental procedure

Flat-plate specimens were fabricated by hot-pressing four aligned laminae which had been formed by arc-spraying [18]. The composite is comprised of 0.20 mm (0.008 in.) diameter 218 CS tungsten fibres with an Fe–22Cr–5.5 Al matrix. The experimentally determined fibre volume fraction is 37%. The as-fabricated composite is well bonded and well densified, with very few voids and good fibre–matrix interfaces (Fig. 5). The plate specimens for 850 and 1000° C were 50 mm wide by 140 mm long (1.97 in. by 5.5 in.), and were mechanically fastened to a conductive plate which is soldered onto a threaded end-grip. The gauge length was 94 mm (3.7 in.). The 1090° C strip specimen was 17.8 mm wide by 140 mm long (0.070 in. by 5.5 in.), and was directly soldered into the threaded end-grip; the gauge length was 86 mm (3.4 in.). Since the threaded end-grip was in a water-cooled block, there

TABLE II Data for 40 vol % W system

T_{MAX} (° C)	$\Delta\varepsilon_p$ (10^{-2})	Relative cycles to equivalent damage
850	1.095	3.25
1000	1.982	1.0
1090	2.523	0.617

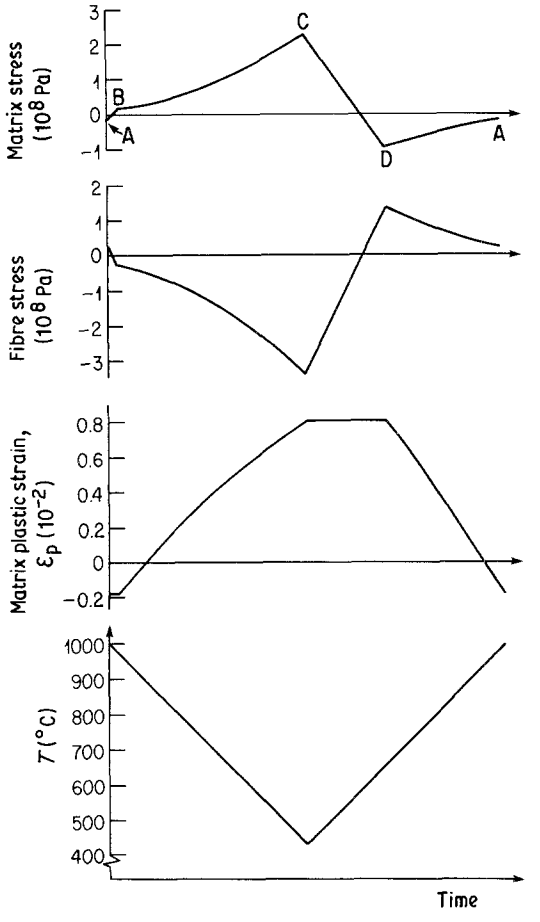

Figure 4 Fibre and matrix cyclic stress; matrix cyclic plastic strain.

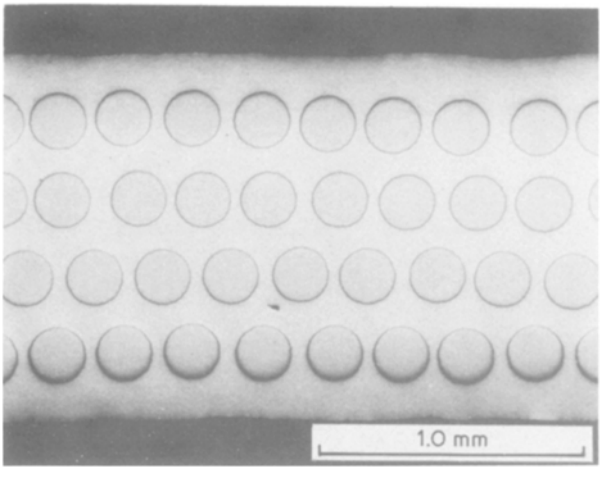

Figure 5 Polished surface of control specimen.

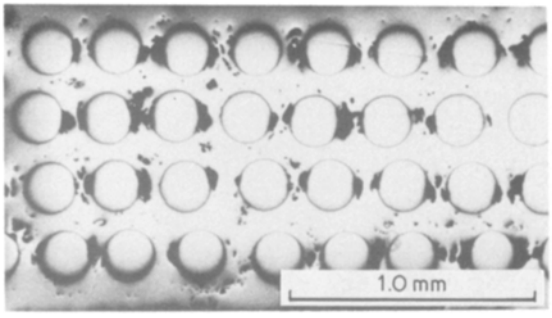

Figure 6 Polished surface of cycled specimen.

was a central hot zone approximately 60, 110 or 90 mm long for the 850, 1000 and 1090° C specimens, respectively. The average specimen thickness is 1.26 mm (0.0498 in.). The hot-zone temperature was verified by an optical pyrometer, and the cycle was controlled by a thermocouple which activated the heating current in an on–off fashion. The temperature variation across the width of the hot section was less than 20° C for the plates, and less than 10° C for the strip. The heat-up time is 30 sec, with cool-down by radiation of 60 to 70 sec for plates, 30 sec for the strip specimen. The loading and unloading rates of the ATS mechanical test machine were adjusted so as to provide virtually no mechanical load during the cycle. The specimen was in an enclosed vacuum chamber to minimize oxidation problems.

5. Experimental results

The specimens were cycled 800 times, with measurement made of the specimen width by micrometer every 100 cycles. The specimen width growth is an indirect measure of matrix damage by void formation; results are given in Table III. The very slight decrease in width for the 850° C specimen illustrates the observed edge oxidation which occurred on all specimens due to an imperfect vacuum.

Tensile strength tests were conducted on 6.4 mm (0.25 in.) wide specimens machined from the tested plate or strip by a diamond-edge cutting wheel. The specimens were dog-boned with a centre gauge section approximately 3.86 mm (0.152 in.) wide by 25 mm (1.0 in.) long. An Instron test machine with wedge-action grips was used, with a head speed of 0.01 in. min^{-1} (0.25 mm min^{-1}). The strength results are given in Table IV.

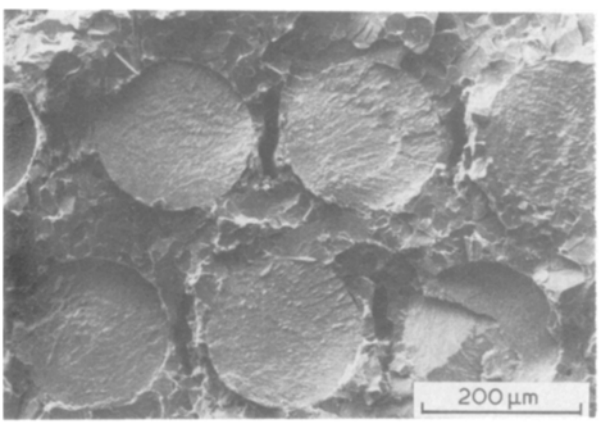

Figure 7 Fracture surface of cycled specimen.

TABLE III Results for cycled specimens

Maximum temperature (° C)	Transverse strain per cycle (10^{-3})
850	−0.38
1000	1.28
1090	7.97

The tungsten wire is ductile as supplied, with a strength in excess of 2000 MPa. After fabrication into a composite, fibres become embrittled due to the formation of an intermetallic reaction zone. Individual fibres were extracted from the matrix by digestion in equal parts of hydrochloric acid, nitric acid and water; this treatment has little effect on the reaction zone. The fibres were held in sandpaper, and gripped with smooth-face pneumatic grips. All fibre behaviour was linear to failure. The control (as-fabricated) fibre strength σ_{fu} was 1480 (+100 −110) MPa with 8 replicates, while the 1000° C fibre strength was 1500 (+170 −100) MPa with 16 replicates. The ranges given show the range of values encountered.

Optical microscopy and SEM photographs of the hot cross-section show an accumulation of matrix damage and void formation for the thermally cycled specimen which were not present in the control (see Figs 6 and 7). We choose the 1090° C specimen as the example for cycled specimens. Fig. 6 shows a polished surface, and Fig. 7 a fracture surface (from a tensile test.) The visible matrix damage seen in Fig. 7 contrasts sharply with the control fracture surface shown in Fig. 8. Another important difference between control and cycled fracture surfaces relates to the fibre–matrix interface, whose reaction zone grows at a stable rate and forms as an intermetallic. The overall thickness of the reaction zone appears the same in the cycled and control specimens, due to the brief time for diffusion at the high temperature. However, the interfacial bond appears to be better for the cycled material, since there is more matrix adhesion to the fibre and less debonding for this material (see Figs 9 and 10). This could promote the propagation of matrix cracks into the fibre.

6. Conclusions

The thermal cycling of a metal-matrix composite whose components have substantially different thermal expansion behaviour can produce large thermal stresses. Thermal cycling without mechanical load is selected as a benchmark worst case for cyclic behaviour. In order to calculate the cyclic stresses and the plastic strain which may lead to damage, we can employ simple micro-mechanical models combined with appropriate constitutive behaviour. The longitudinal stress and

TABLE IV Strength results

Maximum cyclic temperature, T_{MAX} (° C)	Room-temperature tensile strength, σ_{ULT} (MPa (10^3 p.s.i.))	Replicates
Control (uncycled)	772 (112)	3
850	785 (114)	3
1000	655 (95)	2
1090	489 (71)	2

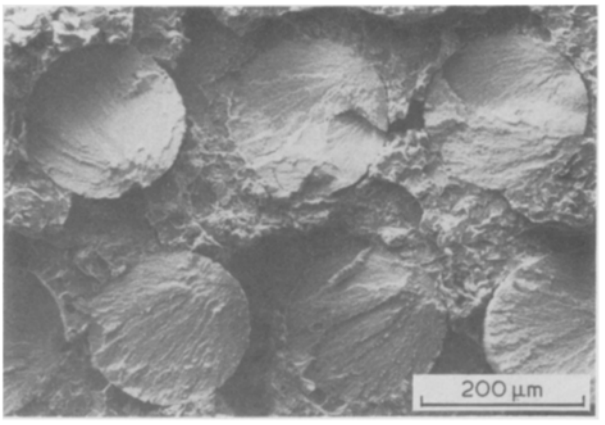

Figure 8 Fracture surface of control specimen.

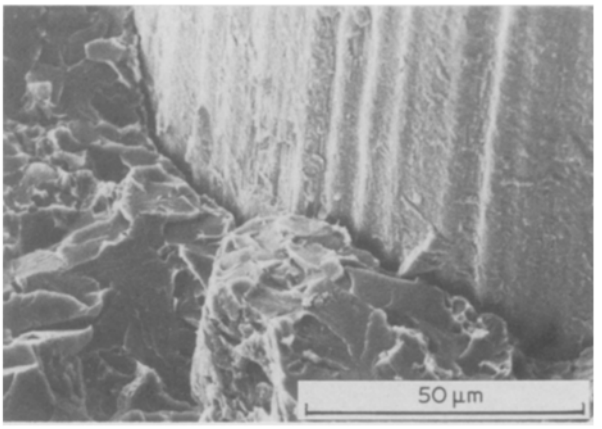

Figure 10 Bonding of control specimen.

strain history for the constitutents of an aligned-fibre composite under thermal cycling may be estimated using the MARC non-linear finite-element program to represent a micro-mechanics strain compatibility model. For this case of rapid thermal cycling, the creep effects are ignored. The results illustrate the large amount of cyclic plastic work experienced by the matrix for a tungsten fibre–Fe CrAlY matrix composite. As the maximum cyclic temperature increases, this work becomes more pronounced due to the rapid decrease in matrix yield stress. Using the Coffin–Manson relationship, a quantitative prediction of the relative matrix damage is proposed. This damage metric has value as a screening tool to determine the best materials for a given thermal cycle, as well as comparing the effect of different thermal cycles on a given material.

The results from thermal cycling tests show agreement with the predicted rapid decline in matrix integrity. The dimensional instability of the width, and the photomicrographs illustrate the growth of matrix damage by void formation. The composite room-temperature tensile strength shows a decline for cyclic temperatures above 850° C, with a decrease in the matrix contribution to the composite strength. That the fibre has not been damaged during cycling, either by fibre plasticity or by growth of the reaction zone, is apparent from the fibre tensile tests. There is also the suggestion that an improved fibre–matrix bond is formed during thermal cycling. This may provide an easier path for matrix cracks to propagate into the fibre, thus lowering the room-temperature strength. Additional support for this is given by the fact that the strength for the 1090° C cycled specimen (489 MPa) is lower than the strength contribution of the fibres alone with no matrix contribution (555 MPa = $\sigma_{fu} V_f$).

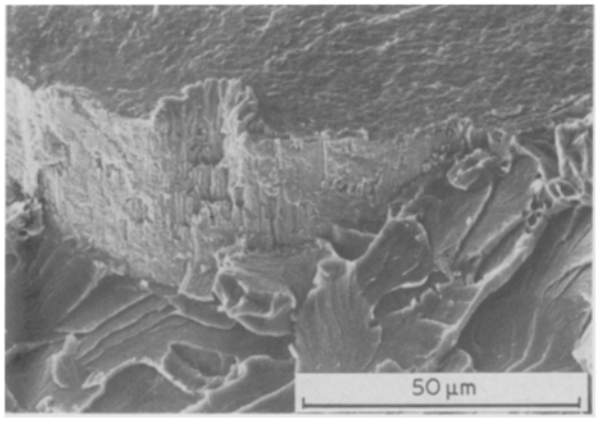

Figure 9 Bonding of cycled specimen.

Acknowledgement

This research was performed under an American Society for Engineering Education Summer Faculty Fellowship while the principal author (R.C.W.) was at NASA–Lewis Research Center. He conveys special gratitude to D. W. Petrasek, D. A. Hopkins and A. Kaufman for their valuable discussions.

References

1. R. A. SIGNORELLI, NASA TM 82929 (1982).
2. *Idem*, NASA TM 83389 (1983) (ITAR, restricted).
3. M. A. WRIGHT, U Tn Space Institute NTIS: AD774890 (1973).
4. M. K. WHITE, M. A. WRIGHT, U Tn Space Institute NTIS: ADA035179 (1976).
5. P. SHAHINIAN, *SAMPE. Q* **2** (1970) 28.
6. G. GARMONG, *Met. Trans.* **5** (1974) 2183.
7. *Idem, ibid.* **5** (1974) 2191.
8. *Idem, ibid.* **5** (1974) 2199.
9. D. BURGREEN, *J. Basic Eng.* **90** (1968) 319.
10. W. R. TYSON, *Met. Trans.* **6A** (1975) 1674.
11. T. E. TIETZ and J. W. WILSON, "Behavior and properties of Refractory Metals" (Stanford University Press, Stanford, 1965) p. 275.
12. R. K. KIRBY, *High Temperature: High Pressures* **4** (1972) 459.
13. D. W. PETRASEK, unpublished communication (1986).
14. "Nickel Base Alloys" (A286) (International Nickel Co., Huntington, W.Va, 1977).
15. C. S. WUKUSICK, GE MP-414, (General Electric, Cincinnati, 1966).
16. L. F. COFFIN Jr, *Trans. ASME* **76** (1954) 931.
17. J. F. TAVERNELLI and L. F. COFFIN Jr, *Trans. ASM* **51** (1959) 438.
18. L. J. WESTFALL, NASA TM 86917 (1985).

Received 18 May
and accepted 22 July 1987